Electronic correlations in Ni 2p and 3p magnetic X-ray dichroism and X-ray photoemission of ferromagnetic nickel

1992 J. Phys.: Condens. Matter 4 4181

(http://iopscience.iop.org/0953-8984/4/16/018)

J. Phys.: Condens. Matter 4 (1992) 4181–4188. Printed in the UK

Electronic correlations in Ni 2p and 3p magnetic x-ray dichroism and x-ray photoemission of ferromagnetic nickel

G van der Laan† and B T Thole‡

† SERC Daresbury Laboratory, Warrington WA4 4AD, UK

‡ Materials Science Centre, University of Groningen, 9747 AG Groningen, Netherlands

Received 16 October 1991

Abstract. The magnetic x-ray dichroism (MXD) in x-ray absorption together with the photoemission of the Ni 2p and 3p levels in ferromagnetic nickel have been analysed using an Anderson impurity model taking into account multiplet splitting. Good agreement with experimental results was obtained for a ground state of 18% d^8, 49% d^9 and 33% d^{10} character. In the Ni 2p MXD the branching ratio and total intensity are determined by the spin–orbit interaction and orbital momentum of the ground state, and the satellite structure results from transitions to a $\underline{p}d^9$ final state.

1. Introduction

The electronic structure and magnetic properties of 3d transition metals have long been an intriguing subject in solid state physics. In particular, this is the case for metallic nickel which has been described by both itinerant and localized models [1]. In a band model, ferromagnetism is explained by a small exchange potential for spin up and spin down. In the Anderson impurity model the ferromagnetic properties can be explained by a small d^8 weight in the ground state. The lowest state of this configuration, the ^3F with parallel spins, imposes a spin alignment on adjacent Ni atoms which fluctuate between $d^9 + d^9$ and $d^{10} + d^8$.

The recently developed technique of magnetic x-ray dichroism (MXD) provides us with a new probe to study the ground state of magnetic materials [2]. In these measurements a core p electron is excited by a dipole transition into the magnetically polarized 3d states. This x-ray absorption process (XAS) is strongly polarization dependent and has recently been studied in detail for 3d transition metals [3]. When the spin of a valence d-hole state is oriented in an exchange field, only core electrons with the same spin orientation can fill this hole. Because the electric vector interacts only with the orbital momentum there is no preference for the excitation of electrons of either spin up or spin down. However, in the presence of spin–orbit interaction, the orbital momentum is coupled to the spin momentum, resulting in a difference in transition probability for up and down spin electrons depending on the polarization of the light. In the absence of electrostatic interactions, a p electron with magnetic quantum number $m = -\frac{3}{2}$ can only be excited into a d state with $m = -\frac{5}{2}$ using right-circularly polarized light ($\Delta m = +1$) [4].

0953-8984/92/164181+08$04.50

The MXD can be calculated either by a one-particle or by a many-electron approach. Local density functional theory, such as a relativistic Korringa–Kohn–Rostoker Green's function method [5–11] as well as multiple scattering theory [12, 13] give a good agreement for rare earth L edges and transition metal K edges. However, a many-body approach is required to explain the multiplet and satellite structures, which are observed in the rare earth M edges and the 3d transition metal L edges [2–4, 14–28].

The magnetic moment of transition metals is composed of a spin and orbital part. Although the orbital contribution is much smaller than the spin contribution, it is important because it determines the anisotropic magnetic properties of the material, such as the magneto-crystalline effect and the easy direction of magnetization [29–31]. There are several experimental techniques which yield information about the orbital magnetic moment, such as neutron diffraction, magnetic x-ray scattering and Compton scattering [32–38]. However, the results are often inconclusive, despite the large amount of effort which is put into these measurements. Recently, we showed that the orbital magnetic moment is equal to the MCD signal integrated over an x-ray absorption edge [28]. This important sum rule can be verified on nickel using the 2p MXD.

The Ni 2p MXD has been measured by Chen *et al* [39] and the Ni 3p MXD by Koide *et al* [40]. The magneto-optical effect in the Ni 3p absorption edge was already predicted by Erskine and Stern [41] using an augmented plane-wave calculation for the 3d band, neglecting electron correlation and spin–orbit interaction. Chen *et al* [42] showed that the main peak in the 2p MXD can be explained using a tight-binding band-structure model with a 3d spin–orbit parameter twice the atomic value. They ascribed the dichroic behaviour of the satellite peaks to many-body effects. The latter was confirmed by Jo and Sawatzky [43, 44] on the basis of an Anderson impurity model with a ground state of 18% d^8, 65% d^9 and 17% d^{10}. X-ray photoemission (XPS) is a more sensitive method to determine the relative d-weights in the ground state [1]. Since the core electron is ejected, the influence of the core-hole potential is larger than in XAS. In this paper we present a combined analysis of the 2p and 3p MXD spectra, together with the XPS spectra, using an Anderson model. We find good agreement for all spectra for a ground state of 18% d^8, 49% d^9 and 33% d^{10}.

2. Calculational details

Consider a particular site in a bulk of Ni atoms with a basis set of states d^8, $d^9\underline{v}$ and $d^{10}\underline{v}^2$, where $\underline{v}$ denotes a combination of appropriate symmetry of orbitals on the adjacent sites. The energies of these basis states are 0, $\Delta - U$ and $2\Delta - U$, respectively, where $\Delta = E(d) - E(v)$ is the transfer energy and U is the d–d Coulomb interaction. The mixing between the basis states in the O_h symmetry of the face-centred-cubic metal is described by e and t_2 parameters [45]. The theory connecting the band and localized descriptions is still unknown and therefore a too great precision in the description of the holes is not justified. However, we feel that in some way we have to take into account that, at least in the initial state without a core hole, the holes are in a specific region of the Brillouin zone. This is of importance for the quenching of orbital momentum and spin–orbit coupling. Because the holes are centred around the L point we describe them in D_{3d} symmetry. The five d functions split into an a_1 and two e representations in D_{3d}. One of the e representations, which

we will call e_1 has e symmetry in O_h, the other one, called e_2, branches from $t_2(O_h)$. These three representations have different hybridization parameters $V(a_1)$, $V(e_1)$ and $V(e_2)$. There is also a cross term $V(e_{12})$ for hopping of an e_1 ligand electron into an e_2 Ni d orbital. A magnetic exchange field along the trigonal axis lifts the Kramers' degeneracy of the d states and reduces the symmetry further to C_{3i}. We will not treat the complication that in some way we have to average over the four L points.

Considering only p to d transitions, the final state configurations $\underline{p}d^9$ and $\underline{p}d^{10}\underline{v}$ in x-ray absorption have relative energies 0 and $\Delta - Q$, respectively, where Q is the p–d Coulomb interaction, and $\underline{p}$ denotes the core hole. The final state configurations $\underline{p}d^8$, $\underline{p}d^9\underline{v}$ and $\underline{p}d^{10}\underline{v}^2$ in x-ray photoemission have relative energies 0 and $\Delta - U - Q$ and $2\Delta - U - 2Q$, respectively. The value of Q in XPS is larger than in XAS, because the effective nuclear charge is increased by one after electron emission. The mixing in the final state is described by the same parameters as in the ground state. The Hamiltonians for the ground and final state, where the exchange field is included by a term $g\mu_B HS$ with $g\mu_B H = -0.5$ eV, are calculated with the Hartree–Fock values of the Slater integrals and the 3d spin–orbit interaction (table 1) reduced to 80% to account for relaxation effects. In principle, these effects can be included by configuration interaction with the low-energy excited configurations, such as in a multi-configurational Dirac–Fock calculation. However, such an approach has little practical advantage in a solid, since there are a large number of small admixtures to the dominant configuration, and a similar result can be obtained by using reduced (scaled) Slater integrals for a single configuration [46]. This scaling results in a reduced multiplet width and a slightly different $L_{2,3}$ branching ratio [47].

The matrix elements were calculated using the chain of groups approach reported by Butler [45]. This approach starts with the calculation of the reduced matrix elements of the necessary operators in the spherical group using Cowan's atomic multiplet program [48]. The Wigner–Eckart theorem is then applied to obtain the reduced matrix elements in the desired point group, where the required isoscalar factors are obtained from Butler's point-group program [45]. The MXD spectrum was obtained as the absorption for right- minus left-circularly-polarized x-rays. Further calculational details are given elsewhere [49].

Good agreement was obtained with experimental results for the parameters $\Delta = -0.75$, $U = 1.50$, $V(a_1) = 1.6$, $V(e_1) = 1.3$, $V(e_2) = 0.8$ and $V(e_{12}) = 0.6$ eV, which produces a $^3A_1$ ground state with 18% d^8, 49% d^9 and 33% d^{10} character. The value of Q was 2.5 in XAS and 4.5 eV in XPS. The spectra were not sensitive to the band width of the d^9 and d^{10} states.

3. $L_{2,3}$ absorption

The experimental XAS spectrum (figure 1, inset) shows L_3 and L_2 peaks with a branching ratio $I(L_3)/[I(L_2) + I(L_3)]$ of 0.72, and a satellite A (A′) at an energy separation of 6.3 eV [39]. The L_3 and L_2 structures have opposite signs in the MXD spectrum where the intensity ratio is −1.6:1. The satellite A (A′) is small in MXD, but a large satellite B (B′) is observed at 3.7 eV, which in the isotropic spectrum is obscured by the tail of the main line.

The calculated spectrum in figure 1 includes only transitions to the 3d shell, which is the reason for the difference with the experimental spectrum, where the high-energy

tail and the platform are due to excitations to the 4s and the continuum states. The L_3 and L_2 structures consist of a main peak with predominantly $\underline{p}d^{10}$ character, and a satellite peak of $\underline{p}d^9$ character. The multiplet structure of the satellite shows a doublet with maxima at the energy positions of peaks B and A. In the experimental XAS, peak A and especially peak A′, are larger than calculated. We assume that there may be extra intensity due to p to s transitions, which were not included in the calculation. The agreement with the experimental spectrum is better in MXD, where the non-magnetic s states are absent. The A and B peaks have a strong dichroism of opposite sign, which is distorted by the tail of the main peak.

The 2p XAS branching ratio depends on the spin–orbit interaction in the ground state. In the isotropic spectrum the branching ratio increases with $\zeta(3d)$ [50], whereas it decreases in the right minus left spectrum. At $\zeta = 0$, the L_3 and L_2 peaks in the MXD have equal intensity but opposite direction, thus the branching ratio goes to infinity. The calculated branching ratios B_{XAS} and B_{MXD} are 0.713 and 2.59, respectively, which are close to the experimental values of 0.72 ± 0.01 and 2.67 ± 0.3. The orbital momentum per hole of the ground state can be obtained from the total intensities using the equation: $\langle L_z \rangle = \frac{2}{3}(I_R - I_L)/I_{iso}$ [28]. The calculated spectrum has a value of 0.053, which is somewhat larger than the experimental spectrum (0.045 assuming $I_{iso} = \frac{1}{2}(I_R + I_L)$), but agrees well with the orbital momentum of 0.054 μ_B measured using neutron diffraction [51] and with the calculated results using a local spin density approximation (LSDA) [29–31].

4. $M_{2,3}$ absorption

The experimental 3p XAS (figure 2, inset) shows a steeply rising edge with weak structures at higher energies [40]. The strongly asymmetric line shape is due to core-hole decay via an autoionization process $3p^63d^n \rightarrow 3p^53d^{n+1} \leftrightarrow 3p^63d^{n-1}\epsilon f$, where ϵf is a continuum state [52]. The experimental MXD shows a large negative peak at the edge. At higher energies there is a small positive background with a dip at 5 eV.

The calculated spectra are given in figure 2, where the core-hole decay has been simulated by a Fano line shape of $\Gamma = 0.8$ eV and $q = 3$ [52]. The XAS spectrum consists of a main line with 80% $\underline{p}d^{10}$ and 20% $\underline{p}d^9$ character, and a satellite at 6 eV with mainly $\underline{p}d^9$ character. The splitting of the main line is caused by the 3p spin–orbit interaction.

The calculated MXD spectrum has a large negative peak at the edge and small oscillations at higher energies. For a pure d^9 ground state, the MXD spectrum would only have a single oscillation with a breadth equal to the 3p spin–orbit splitting. However, the interference with the $3\underline{p}d^9$ final state changes the upper part of this oscillation. The influence of the spin–orbit interaction is clearly visible in the total intensity of the MXD spectrum; when $\zeta(3d) = 0$ the total intensity is zero (figure 2(*c*)).

5. Photoemission

The Ni 2p and 3p XPS spectra are shown in figures 3 and 4. They consist of a main peak with primarily $\underline{p}d^{10}$ and a satellite structure with primarily $\underline{p}d^9$ character. The satellite intensity, which is 38% in figure 3, is strongly dependent on the difference in

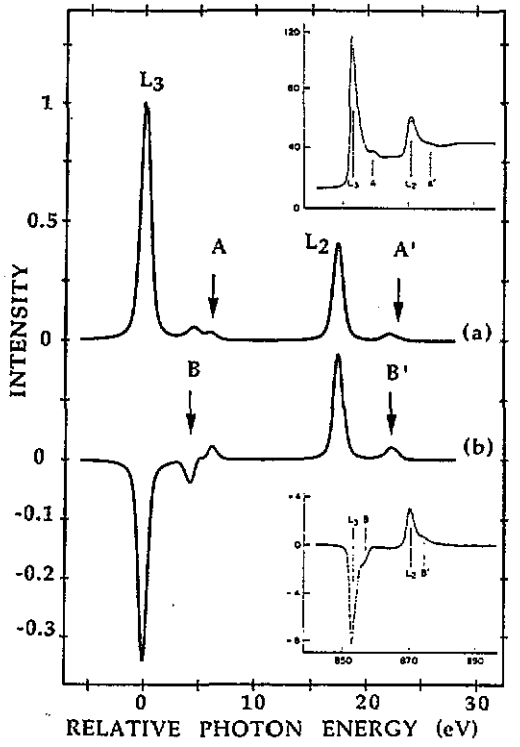

Figure 1. Calculated Ni 2p absorption spectrum of ferromagnetic nickel for: (*a*) isotropic; (*b*) right-minus left-circularly-polarized x-rays. A (A') and B (B') give the positions of the satellite peaks observed in the experimental spectrum (inset, [39]). Convolution by a Lorentzian $\Gamma = 0.24$ eV and Gaussian lineshape $\sigma = 0.32$ eV.

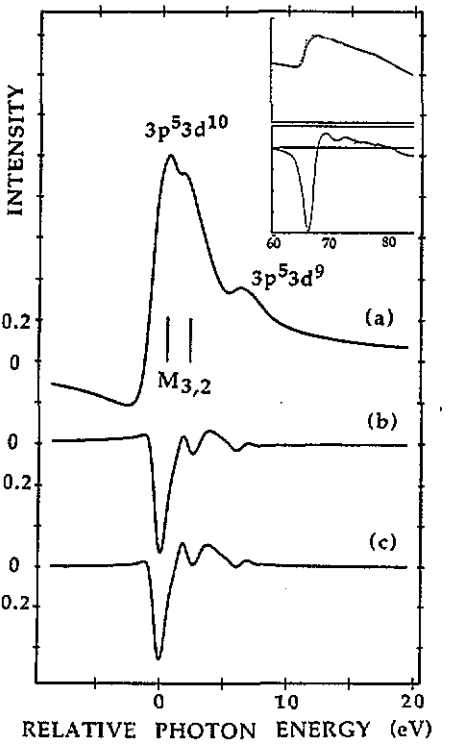

Figure 2. Calculated Ni 3p absorption spectrum of ferromagnetic nickel for: (*a*) isotropic; right-minus left-circularly-polarized x-rays; (*b*) with and (*c*) without 3d spin–orbit interaction. Convolution by a Fano lineshape $\Gamma = 0.8$ eV and $q = 3$. The inset shows the experimental right and left spectrum (upper) and the asymmetry (lower panel) from [40].

hybridization between the initial and final state [53]. Since the final states have rather pure characters, the satellite intensity increases with the amount of d^9 character in the ground state. In the experimental spectra [54] the satellite structures are broadened compared with the main peaks due to additional decay channels. In the 3p spectrum (figure 4) the electrostatic interactions are larger than the core-hole spin–orbit interaction (table 1). The $3\underline{p}d^9$ state is split into three clearly distinguishable structures, $^3F^1D$, $^3P^3D$ and $^1P^1F$.

6. Conclusions

We have shown that the observed Ni 2p and 3p MXD can be explained using an Anderson impurity model with a ground state of 18% d^8, 49% d^9 and 33% d^{10}. These d-weights have been verified using XPS spectra. Although the qualitative spectral shape remains the same over a relatively large range of d-weights, the relative

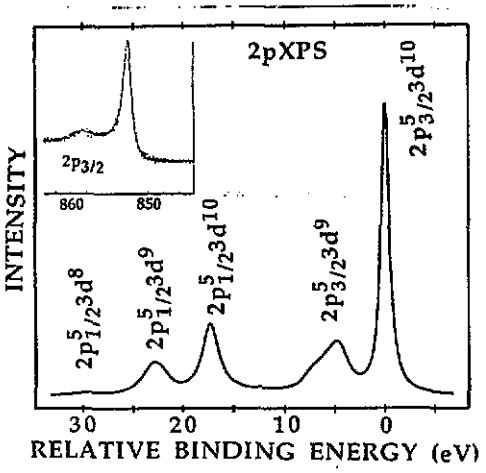

Figure 3. Calculated Ni 2p XPS of ferromagnetic nickel. Convoluted by a Lorentzian lineshape $\Gamma = 0.5$ (first peak), 1 eV. The inset shows the experimental spectrum [54].

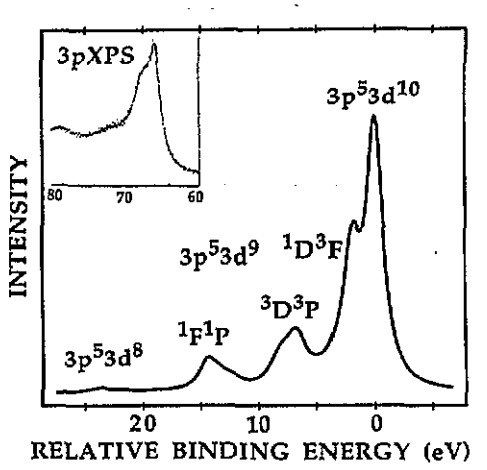

Figure 4. Calculated Ni 3p XPS of ferromagnetic nickel. Convolution by a Lorentzian lineshape $\Gamma = 0.8$ eV. The inset shows the experimental spectrum [54].

Table 1. The *ab initio* values (eV) of the parameters in the Hartree–Fock calculation for the initial- and final-state configurations in XAS and XPS as obtained by Cowan's code [48]. The actual values of these parameters, except the core-hole spin–orbit interaction, have been scaled to 80% in the calculation.

Configuration	F^2(d,d)	F^4(d,d)	ζ(p)	ζ(3d)	F^2(p,d)	G^1(p,d)	G^3(p,d)
Ni $3d^8$	12.234	7.597	—	0.083	—	—	—
Ni $3d^9$	—	—	—	0.074	—	—	—
Ni $2p^53d^8$	14.023	8.761	11.506	0.112	8.349	6.332	3.603
Ni $2p^53d^9$	—	—	11.507	0.102	7.721	5.787	3.291
Ni $2p^53d^{10}$	—	—	11.509	—	—	—	—
Ni $3p^53d^8$	13.317	8.319	1.397	0.092	14.333	17.717	10.798
Ni $3p^53d^9$	—	—	1.366	0.084	13.633	16.900	10.277
Ni $3p^53d^{10}$	—	—	1.345	—	—	—	—

intensities and energy positions change considerably. We found that a ground state with more d^9 character also gives a good agreement for MXD, but a worse agreement for XPS. A ground state such as that proposed by Jo and Sawatzky [43] with 65% d^9 results in XPS spectra with much larger satellite intensity. The analysis of the MXD spectra confirms the earlier predictions from the 2p XAS branching ratio [50] about the presence of spin–orbit interaction in the ground state. The orbital momentum was obtained from the total intensity of the MXD spectrum.

Acknowledgments

We are grateful to George Sawatzky, Francesco Sette and Paolo Carra for valuable discussions.

References

[1] Davis L C 1986 *J. Appl. Phys.* **59** R25 and references therein
[2] van der Laan G, Thole B T, Sawatzky G A, Goedkoop J B, Fuggle J C, Esteva J M, Karnatak R C, Remeika J P and Dabkowska H A 1986 *Phys. Rev.* B **34** 6529
[3] van der Laan G and Thole B T 1991 *Phys. Rev.* B **43** 13401
[4] van der Laan G and Thole B T 1990 *Phys. Rev.* B **42** 6670
[5] Ebert H, Strange P and Gyorffy B L 1988 *J. Appl. Phys.* **63** 3055
[6] Ebert H, Strange P and Gyorffy B L 1988 *Z. Phys.* B **73** 77
[7] Collins S P, Cooper M J, Brahmia A, Laundy D and Pitkanen T 1989 *J. Phys. C: Solid State Phys.* **1** 323
[8] Ebert H and Zeller R 1989 *Physica* B **161** 191
[9] Ebert H, Drittler B, Zeller R and Schütz G 1989 *Solid State Commun.* **69** 485
[10] Ebert H and Zeller R 1990 *Phys. Rev.* B **42** 2744
[11] Baudelet F, Dartyge E, Fontaine A, Brouder C, Krill G, Kappler J P and Piecuch M 1991 *Phys. Rev.* B **43** 5857
[12] Brouder C and Hikam M 1991 *Phys. Rev.* B **43** 3809
[13] Natoli C R unpublished
[14] Thole B T, van der Laan G and Sawatzky G A 1985 *Phys. Rev. Lett.* **55** 2086
[15] van der Laan G 1987 *Giant Resonances in Atoms, Molecules and Solids (NATO Advanced Study Institute Series B: Physics)* vol 151 ed J P Connerade (New York: Plenum) p 447
[16] Goedkoop J B, Fuggle J C, Thole B T, van der Laan G and Sawatzky G A 1988 *J. Appl. Phys.* **64** 5595
[17] Goedkoop J B, Thole B T, van der Laan G, Sawatzky G A, de Groot F M F and Fuggle J C 1988 *Phys. Rev.* B **37** 2086
[18] Jo T and Imada S 1989 *J. Phys. Soc. Jpn.* **58** 1922
[19] van der Laan G 1990 *Phys. Scr.* **41** 574
[20] van der Laan G 1990 *Proc. 2nd European Conf. Progress in X-Ray Synchrotron Radiation Research* vol 25, ed A Balerna, E Bernieri and S Mobilio (Bologna: SIF) p 243
[21] Imada S and Jo T 1990 *J. Phys. Soc. Japan* **59** 3358
[22] Sette F, Chen C T, Ma Y, Modesti S and Smith N V 1990 *AIP Conf. Proc.* vol 215 p 787
[23] Carra P and Altarelli M 1990 *Phys. Rev. Lett.* **64** 1286
[24] Carra P, Harmon B N, Thole B T, Altarelli M and Sawatzky G A 1991 *Phys. Rev. Lett.* **66** 2495
[25] Sacchi M, Sakho O and Rossi G 1991 *Phys. Rev.* B **43** 1276
[26] Jo T 1992 *Synchrotron Radiation News* **5** 21
[27] Imada S and Jo T *J. Magn. Magn. Mat.* to be published
[28] Thole B T, Carra P, Sette F and van der Laan G 1992 *Phys. Rev. Lett.* submitted
[29] Ericksson O, Johansson B, Albers R C, Boring A M and Brooks M S S 1990 *Phys. Rev.* B **41** 11807
[30] Ericksson O, Nordström L, Pohl A, Severin L, Boring A M and Johansson B 1990 *Phys. Rev.* B **41** 11807
[31] Ericksson O, Fernando G W, Albers R C and Boring A M 1991 *Solid State Commun.* **78** 801
[32] Blume M 1985 *J. Appl. Phys.* **57** 3615
[33] Blume M and Gibbs D 1988 *Phys. Rev.* B **37** 1779
[34] Gibbs D, Harshmann D R, Isaacs E D, McWhan D B, Mills D and Vettier C 1988 *Phys. Rev. Lett.* **61** 1241
[35] McWhan D B, Vettier C, Isaacs E D, Ice G E, Siddons D P, Hastings J B, Peters C and Vogt O 1990 *Phys. Rev.* B **42** 6007
[36] Lovesey S W 1991 *Phys. Scr.* **44** 51
[37] Lander G H 1991 *Phys. Scr.* **44** 33
[38] Stirling W G, Cooper M J and Pattison P (ed) 1991 Magnetic x-ray scattering *(Daresbury Scientific Report Series R30)*
[39] Chen C T, Sette F, Ma Y and Modesti S 1990 *Phys. Rev.* B **42** 7262
[40] Koide T, Shidara T, Fukutani H, Yamaguchi K, Fujimori A and Kimura S 1991 *Phys. Rev.* B **44** 4697
[41] Erskine J L and Stern E A 1975 *Phys. Rev.* B **12** 5016
[42] Chen C T, Smith N V and Sette F 1991 *Phys. Rev.* B **43** 6785
[43] Jo T and Sawatzky G A 1991 *Phys. Rev.* B **43** 8771
[44] Yoshida A and Jo T 1991 *J. Phys. Soc. Japan* **60** 2098
[45] Butler P H 1981 *Point Group Symmetry, Applications, Methods and Tables* (New York: Plenum)
[46] Lynch D W and Cowan R D 1987 *Phys. Rev.* B **36** 9228

[47] Thole B T and van der Laan G 1988 *Phys. Rev.* B **38** 3158
[48] Cowan R D 1981 *The Theory of Atomic Structure and Spectra* (Berkeley: University of California Press)
[49] Thole B T and van der Laan G 1991 *Phys. Rev.* B **44** 12424
[50] van der Laan G and Thole B T 1988 *Phys. Rev. Lett.* **60** 1977
[51] Brown P J *et al* 1992 unpublished
[52] Davis L C and Feldkamp L A 1976 *Solid State Commun.* **19** 413
[53] van der Laan G, Westra C, Haas C and Sawatzky G A 1981 *Phys. Rev.* B **23** 4369
[54] Hüfner S and Wertheim G K 1975 *Phys. Lett.* **51A** 299, 301